Growth potential of high aspect ratio elliptic delaminations

P. Czarnocki[1]

[1] Institute of Aeronautics and Applied Mechanics, Warsaw University of Technology

ABSTRACT: *Behaviour of the embedded elongated elliptic delamination was studied using FEM. The magnitudes and distributions of G_I, G_{II} and G_{III} along a delamination front were determined with the help of the Modified Crack Closure Integral Method. The non-linearity resulting from both the large rotations of delaminated sub-laminate and contact between delamination separated layers were taken into account. The results showed that the contact conditions and location of the contact regions change significantly with loading. Such changes affect the magnitude, proportions and distribution of G_I, G_{II} and G_{III} along the delamination front. Also, the results suggest that, perhaps, it could be possible to make rough estimation of the hazard level that an elliptic delamination produces by making calculations for a circular delamination of radius equal to the minor axis of the ellipse in question.*

INTRODUCTION

Typical embedded delaminations can result from imperfect manufacturing process or low energy impact. The presented analysis focuses on the former, however, if only the constitutive relationships for impact damaged composite are known the same approach can be applied to the latter. Once the delamination has been detected an important question arises about the hazard level it involves. It can be estimated by calculating the magnitudes and distributions of G_I, G_{II} and G_{III} along a delamination front. Solution to the problem usually involves two steps. In the first one post buckling solution is obtained for the delaminated sublaminate and in the second one the Strain Energy Release Rate, (SERR), components are calculated along the delamination border for the deformed laminate. Several papers dealing with this problem have been published. Assuming an important role of buckling strains in the delamination phenomenon Shivakumar [1] analysed buckling strains of elliptic embedded delamination with the use of Rayleigh-Ritz method and Von-Karman strain-displacement relationships as well as with FEM. Whitcomb [2] analysed circular end elliptical delaminations with the help of FEM and simplified fracture analysis. He provided relationships

between strains and G_I and G_{II} in the form of graphs for specific locations defined by azimuth $\alpha=0°$ and $\alpha=90°$ measured relative to the loading direction. In [3] the effect of possible contact between disbonded layers on the magnitude and distribution of the SERR components was analysed. Chai [4,5] carried out similar analyses. He also applied the Rayleigh-Ritz method with the Von-Karman strain-displacement relationships to obtain a post-buckling solution. Then, he estimated the SERR components on the basis of previously calculated membrane stresses and bending moments, (the method used is presented in detail e.g. in [6]. It requires the assumption of plane strain state in the plane perpendicular to the delamination). Yin [7] and Jane [8] presented the same approach as in [5], however, they used higher order polynominals and claimed more accurate results. Czarnocki [9] analysed the effect of reinforcement arrangement on buckling load, and distribution and proportions of the SERR components for circular delaminations. The applied non-linear FE model took into account contact between disbanded layers. More recently, also using FEM, Shen et al. [10] and Riccio et al. [11] studied the dependence of SERR on the thickness of delaminated layer for circular delaminations.

All the papers known to the author deal with circular or low aspect ratio elliptic delaminations in case when changes in buckling mode do not occur during loading. However, for elliptic delaminations of high aspect ratio such a phenomenon takes place and is followed by changes in location and size of contact area. The work presented is focussed on these problems as well as on comparison of the results obtained for elliptic and circular delaminations.

ANLYSIS

For analysis purpose the elliptic delamination of aspect ratio equal to 5 embedded in an orthotropic rectangular plate was taken into consideration. A compressive loading applied to the sides of the plate acted in the direction parallel to the major ellipse axis. The lamina partially disbanded from the core and the core constituted cross-ply laminate i.e. reinforcement directions of the former and the latter were rotated with respect to each other by 90°. Two cases of the reinforcement arrangement were considered (i) reinforcement of the delaminated layer aligned with the loading direction, (ii) reinforcement of the delaminated layer perpendicular to the loading direction. The analysis was divided into two steps. In the first one the linear buckling analysis was performed to estimate the critical load causing the

local buckling of delaminated layer and to define the regions of possible overlap. In the second step the non-linear buckling and post-buckling analysis was carried out. It took into account the changes in contact caused by load increase. Finally, the results obtained were post processed using the Modified Crack Closer Integral Method, (MCCIM), [12], to analyse the changes in magnitude, proportions and distribution of G_I, G_{II} and G_{III}. Analysis for circular delaminations was carried out in the same manner. The FE model used was described in [9].

Structure

The geometry and loading conditions of the analysed structure are shown in Figure 1. The elliptic delamination of aspect ratio a/b=5 and the length of major ellipse axis 2a =200 mm was embedded in 100x300 mm rectangular plate. The total thickness of the plate H and delaminated layer, h were 5 mm and 0.5 mm, respectively. The assumed elastic properties of the delaminated layer and core were typical of highly orthotropic material, i.e. UD CFRP. It was assumed that the ellipse axes and the principle material directions coincide. The elastic constants assumed in the case considered were as follow: E_{11}=130GPa, E_{22}=E_{33} =0.97GPa, G_{12}=G_{13}=0.54GPa, G_{23}=0.31GPa, μ_{12}=μ_{13} =0.29, μ_{23}=0.36.
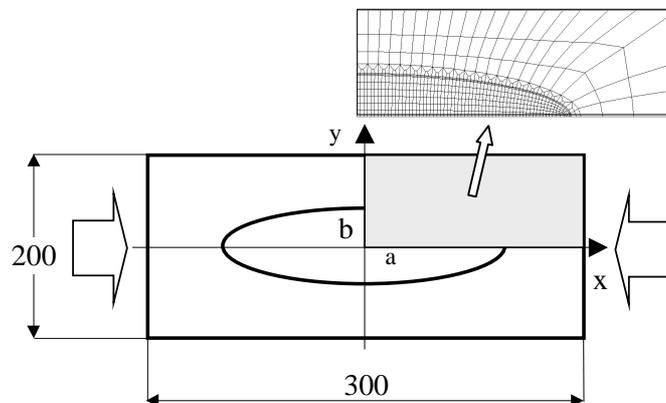
Figure 1: Analysed structure and its finite element representation

Finite Element Model

The basic calculations were made with the help of ANSYS 54 finite element code. To simplify the post-processing procedure used for the mode partition and calculation of G_I, G_{II} and G_{III} with the help of MCCIM the mesh was design in such a way that its lines crossed each other approximately at 90°

in the vicinity of the delamination border. Due to the symmetry with the respect to xz and yz planes it was sufficient to model a quarter of the structure. The plate was subjected to uniaxial compressive loading by forcing uniform displacement of its opposite sides in the x direction. To avoid global buckling the symmetry boundary conditions with the respect to xy plane were applied. The model was built with the eight node anisotropic brick elements SOLID 64. In the regions were penetration was expected the point-to-surface CONTACT 49 elements of contact stiffness 20000 kN/mm were applied. The choice of the appropriate regions for application of these elements was based on the results obtained from the linear buckling analysis. To obtain nodal forces closing the gap, the adjacent nodes of the delamination separated surfaces were connected with the COMBIN 14 spring elements. The crack length to close was equal to 0.25 mm. The values of SERR were calculated at 65 points uniformly distributed along the delamination front.

RESULTS AND DISCUSSION

Figure 2 depicts the first buckling modes for the elliptic and circular delamination, as obtained from the linear buckling analysis. For the former three buckle half wavelengths are present while for the latter just one. The same pattern occurs for the both reinforcement arrangements.


Figure 2: First buckling modes for (a) elliptic and (b) circular delaminations. The profiles are shown in a plane parallel to the loading direction

Figures 3 and 4 present profiles of the out of plane deformations in y=0 planes for elliptic delaminations, as obtained from the non-linear buckling analysis. The effect of contact is clearly visible. The profiles represent deformation for ε_x=-0.003 and ε_x=-0.001 loading levels for reinforcement arrangement used in case (i) and for ε_x=-0.0055 and ε_x=-0.01 loading levels for the reinforcement arrangement used in case (ii). In the latter, ε_x=-0.0055 produced out of plane displacement u_z≈0.05mm. Due to relatively low value of u_z this strain was arbitrary assumed to be just above the critical one.

Figure 4 depicts top views of the buckled delaminations. It can be seen that the highest bulges occur approximately in the same location independently of loading level.
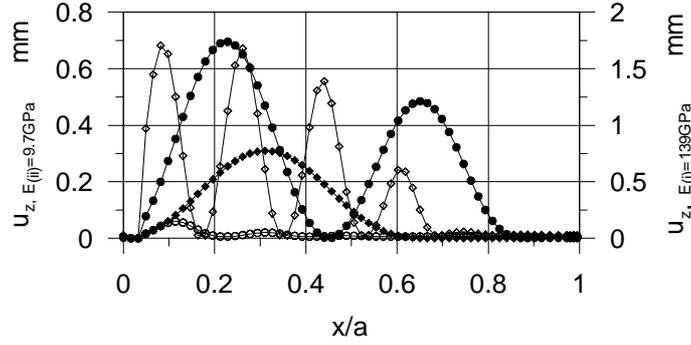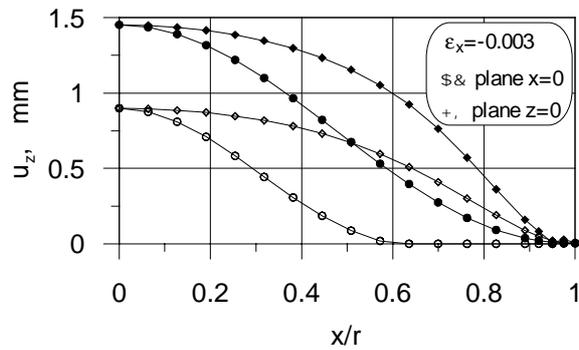

Figure 3: Profiles of the out of plane displacements for elliptic delaminations in y=0 plane. The close symbols correspond to case (i), the open ones to case (ii).
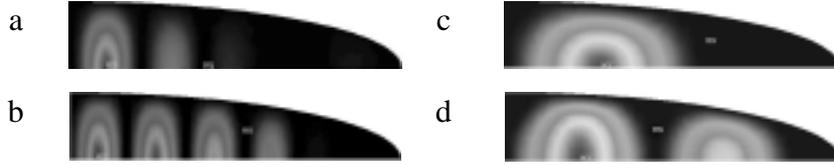

Figure 4: Top views of the buckled delamination layers (a, b) for $E_{(ii)}$=9.7GPa, and (c, d) for $E_{(i)}$ =1390GPa, (a) and (b) correspond to the plots with open symbols, and (c), and (d) to the plots with close ones shown in Figure 3.

For comparison purpose the profiles for the circular delaminations corresponding to cases (i) and (ii) of the reinforcement arrangement at ε_x=-0.003 are shown in figure 5. Figure 6 depicts changes in magnitude and proportions of the SERR depending on location. The same relationships for the elliptic delaminations are shown in figure 7. It can be noticed that for elliptic delaminations in all the cases considered the SERR reaches maximum in the neighbourhood of the intersection of the delamination front with x=0 plane and for circular ones at the intersection. For elliptic delaminations G_{II} components dominate. For circular delaminations components G_{II} and G_I are of similar magnitude. For the both delamination shapes G_{III} component is negligible. For case (ii) SERR values for circular

delamination are higher than for the elliptic one despite the difference in loading level.
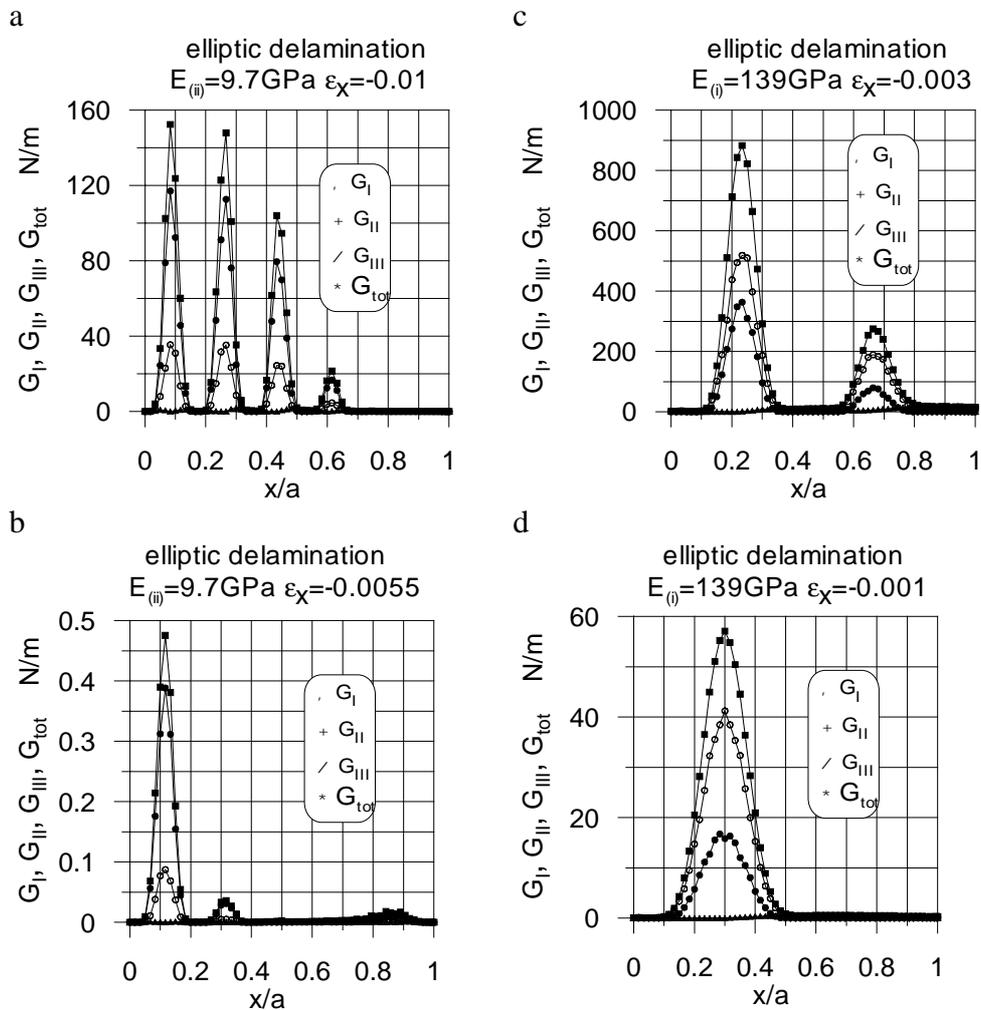

Figure 5: Profiles of the out of plane displacements for circular delaminations; open symbols for $E_{(ii)}$=9.7GPa, close symbols for $E_{(i)}$=139GPa
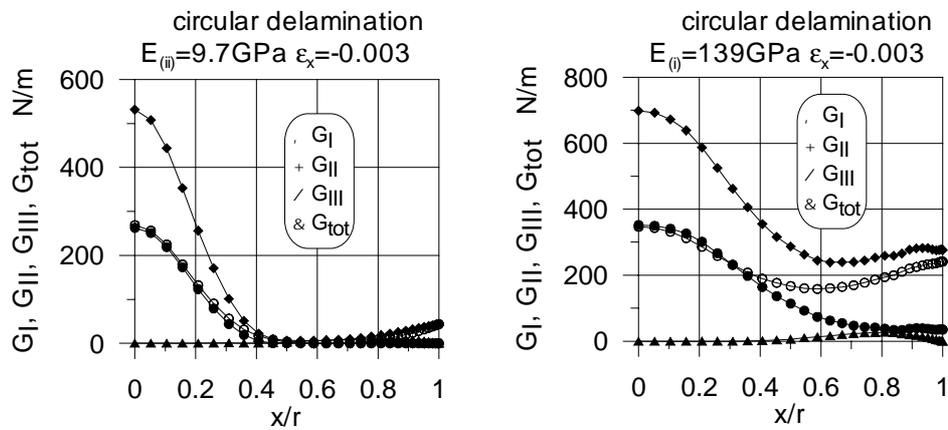
Figure 6: Variation of G_I, G_{II} G_{III} and G_{tot} vs. x/r for circular delaminations

In case (i) for the same loading level G_{II} is higher for elliptic delamination while G_I for the both delamination shapes take similar values. Taking into account fact that for typical laminates G_{IIc} is much higher than G_{Ic}, [13], one can suggest that hazard levels produced by the circular delamination and the elliptic one are similar provided that the radius of circular delamination and

the minor ellipse axis of the elliptic delamination in question are of the same length.

a

elliptic delamination
$E_{(ii)}=9.7GPa$ $\varepsilon_X=-0.01$

c

elliptic delamination
$E_{(i)}=139GPa$ $\varepsilon_X=-0.003$

b

elliptic delamination
$E_{(ii)}=9.7GPa$ $\varepsilon_X=-0.0055$

d

elliptic delamination
$E_{(i)}=139GPa$ $\varepsilon_X=-0.001$

Figure 7: Variation of G_I, G_{II} G_{III} and G_{tot} vs. x/a for elliptic delamination.

CONCLUSIONS

The following conclusions can be drown:
- Perhaps, it could be possible to make rough estimation of the hazard level that an elliptic delamination produces by making calculations for a circular delamination of radius equal to the minor axis of the ellipse in

question. However, to justify the hypothesis further investigations are needed
- Increase in loading level produces changes in contact conditions which in turn significantly affect distribution of SERR components along the delamination front
- For elliptic delaminations compressed along their major axes G_{II} component dominates while for circular delaminations components G_I and G_{II} are comparable.
- G_{III} component is negligible

REFERENCES

1. Shivakumar, K.N., Whitcomb, J.D. (1985) *Journal of Composite Materials* **19**, 2.
2. Whitcomb, J.D. (1990) pp.215-230 In*: Composite Materials: Testing and Design, ASTM STP 1059* Garbo S.P. (Ed.) A.S.T.M. Philadelphia
3. Whitcomb, J.D. (1992) *Journal of Composite Materials* **10**, 1523
4. Chai, H., Babcock, C.D. (1984) *Journal of Composite Materials* **19**, 67.
5. Chai, H., (1990) *International Journal of Fracture* **46**, 237
6. Yin, W.L., and Wang, T.S. (1984) *Journal of Applied Mechanics* **51**, 939.
7. Yin, W.L., Jane K.C. (1992) *International Journal of Solids and Structures* **29,** 591.
8. Jane, K.C., Yin W.L. (1992) *International Journal of Solids and Structures* **29,** 611.
9. Czarnocki, P. (2000). In: *Fracture of Polymers, Composites and Adhesives*, pp.49-60, Williams J.G. and Pavan A., (Ed). ESIS Publication 27.
10. Shen, F., Lee, K.H., Tay, T.E. (2001) *Composite Science and Technology* **61**, 1241.
11. Riccio, A., Scaramuzzino, F., Perugini, P. (2001) *Composites: Part B* **32**, 209.
12. Rybicki, E.F., Kanninen, M.F. (1977) *Engineering Fracture Mechanics* **9**, 931.
13. Bradly, W.L. (1989). In: Application of Fracture Mechanics to Composite Materials, pp.174-186, Friedrich, K., (Ed.). Elsevier Science Publishers B.K., The Netherlands.